

Impact of velocity distribution assumption on simplified laser speckle imaging equation

Julio C Ramirez-San-Juan^{a*}, Ruben Ramos-Garcia^a, Ileana Guizar-Iturbide^a, Gabriel Martinez-Niconoff^a, and Bernard Choi^{b,c}

^aOptics Department, Instituto Nacional de Astrofísica, Óptica y Electrónica, Luis Enrique Erro No. 1, Puebla, 72840, México

^bBeckman Laser Institute and Medical Clinic, University of California, Irvine, 1002 Health Sciences Road East, Irvine, CA 92612, USA

^cDepartment of Biomedical Engineering, University of California, Irvine, CA 92612, USA

*Corresponding author: jcram@inaoep.mx

Abstract: Since blood flow is tightly coupled to the health status of biological tissue, several instruments have been developed to monitor blood flow and perfusion dynamics. One such instrument is laser speckle imaging. The goal of this study was to evaluate the use of two velocity distribution assumptions (Lorentzian- and Gaussian-based) to calculate speckle flow index (SFI) values. When the normalized autocorrelation function for the Lorentzian and Gaussian velocity distributions satisfy the same definition of correlation time, then the same velocity range is predicted for low speckle contrast ($0 < C < 0.6$) and predict different flow velocity range for high contrast. Our derived equations form the basis for simplified calculations of SFI values.

©2007 Optical Society of America

OCIS codes: (120.6150) Speckle imaging; (120.7250) Velocimetry; (170.3340) Laser Doppler velocimetry; (999.9999) Blood flow velocity.

References

1. A. K. Dunn, T. Bolay, M. A. Moskowitz and D. A. Boas, "Dynamic imaging of cerebral blood flow using laser speckle," *J. Cereb. Blood Flow Metab.* **21**, 195-201 (2001).
2. S. A. Sheth, M. Nemoto, M. W. Guiou, M. A. Walker and A. W. Toga, "Spatiotemporal evolution of functional hemodynamic changes and their relationship to neuronal activity," *J. Cereb. Blood Flow Metab* **25**, 830-841 (2005).
3. H. W. Ren, Z. H. Ding, Y. H. Zhao, J. J. Miao, J. S. Nelson and Z. P. Chen, "Phase-resolved functional optical coherence tomography: simultaneous imaging of in situ tissue structure, blood flow velocity, standard deviation, birefringence, and Stokes vectors in human skin," *Opt. Lett.* **27**, 1702-1704 (2002).
4. Z. P. Chen, T. E. Milner, D. Dave and J. S. Nelson, "Optical Doppler tomographic imaging of fluid flow velocity in highly scattering media," *Opt. Lett.* **22**, 64-66 (1997).
5. A. F. Fercher and J. D. Briers, "Flow Visualization by Means of Single-Exposure Speckle Photography," *Opt. Commun.* **37**, 326-330 (1981).
6. J.D. Briers and S. Webster, "Quasi real-time digital version of single-exposure speckle photography for full-field monitoring of velocity or flow fields," *Opt. Commun.* **116**, 36-42 (1995).
7. J. D. Briers, G. Richards and X. W. He, "Capillary blood flow monitoring using laser speckle contrast analysis (LASCA)," *J. Biomed. Opt.* **4**, 164-175 (1999).
8. H. Y. Cheng, Q. M. Luo, S. Q. Zeng, S. B. Chen, J. Cen and H. Gong, "Modified laser speckle imaging method with improved spatial resolution," *J. Biomed. Opt.* **8**, 559-564 (2003).
9. H. Y. Cheng, Q. M. Luo, S. Q. Zeng, S. B. Chen, W. H. Luo and H. Gong, "Hyperosmotic chemical agent's effect on in vivo cerebral blood flow revealed by laser speckle," *Appl. Opt.* **43**, 5772-5777 (2004).
10. S. Yuan, A. Devor, D. A. Boas and A. K. Dunn, "Determination of optimal exposure time for imaging of blood flow changes with laser speckle contrast imaging," *Appl. Opt.* **44**, 1823-1830 (2005).
11. A. K. Dunn, A. Devor, A. M. Dale and D. A. Boas, "Spatial extent of oxygen metabolism and hemodynamic changes during functional activation of the rat somatosensory cortex," *Neuroimage* **27**, 279-290 (2005).
12. H. Bolay, U. Reuter, A.K. Dunn, Z.H. Huang, D.A. Boas, M.A. Moskowitz, "Intrinsic brain activity triggers trigeminal meningeal afferents in a migraine model," *Nat. Med.* **8**, 136-142 (2002).

13. M. Hirao, H. Oku, W. Goto, T. Sugiyama, T. Kobayashi and T. Ikeda, "Effects of adenosine on optic nerve head circulation in rabbits," *Exp. Eye Res.* **79**, 729-735 (2004).
14. K. R. Forrester, J. Tulip, C. Leonard, C. Stewart and R. C. Bray, "A laser speckle imaging technique for measuring tissue perfusion," *IEEE Trans. Biomed. Eng.* **51**, 2074-2084 (2004).
15. B. Choi, N. M. Kang and J. S. Nelson, "Laser speckle imaging for monitoring blood flow dynamics in the in vivo rodent dorsal skinfold model," *Microvasc. Res.* **68**, 143-146 (2004).
16. T. K. Smith, B. Choi, J. C. Ramirez-San-Juan, J. S. Nelson, K. Osann and K. M. Kelly, "Microvascular blood flow dynamics associated with photodynamic therapy and pulsed dye laser irradiation," *Lasers Surg. Med.*, **38**, 532-539 (2006).
17. B. Choi, J.C. Ramirez-San-Juan, J. Lotfi, J.S. Nelson, "Linear response range characterization and in vivo application of laser speckle imaging of blood flow dynamics," *J. Biomed. Opt.* **11**, 041129 (2006).
18. H. Cheng and T.Q. Duong; "Simplified laser-speckle-imaging analysis method and its application to retinal blood flow imaging," *Opt. Lett.* **15**, 2188-2190 (2007).
19. P. Zakharov, A. Völker, A. Buck, B. Weber and F. Scheffold; "Quantitative modeling of Laser Speckle Imaging," *Opt. Lett.* **31**, 3465-3467 (2006).
20. J. W. Goodman, *Statistical Optics* (John Wiley & Sons, 1985).
21. J.W. Goodman, "Some effects of target-induced scintillation on optical radar performance," *Proc. IEEE*, **53**, 1688 (1965).
22. J.D. Briers and A.F. Fercher "A laser speckle technique for the visualization of retinal blood flow," *Proc. SPIE* **369**, 22-28 (1982).
23. R. Bracewell, *The Fourier transform and its applications* (Mc Graw-Hill, 1965).

1. Introduction

Noninvasive monitoring of a therapeutic intervention is desired to provide the clinician or scientist with insight into the efficacy of the treatment. Since blood flow is tightly coupled into the health status of biological tissue, several instruments have been developed to monitor blood flow and perfusion dynamics, including laser Doppler flowmetry [1,2] and Doppler optical coherence tomography [3,4].

Fercher and Briers [5] proposed a technique for flow visualization by means of single-exposure photography. It uses the spatial statistics of time-integrated speckle (essentially the speckle contrast) and was originally developed for the measurement of retinal blood flow. Recently, this laser speckle imaging (LSI) method has been developed into a digital, quasi real-time technique for the mapping of blood flow [6,7]. LSI has been used to monitor noninvasively blood flow and perfusion dynamics in the brain [1,8-12], retina [5,13], and skin [14-17]. We have employed LSI to monitor blood flow dynamics during photodynamic therapy [16] and have observed marked changes in the measured speckle flow index (SFI) values which is proportional to the blood flow velocity. Cheng and Duong [18] recently proposed a simplified imaging equation that addresses a reported discrepancy [19] between the Fercher and Briers speckle imaging equation and that of Goodman [20, 21]. The authors proposed that this equation is valid for $T/\tau_c > 100$, where T is image exposure time and τ_c is speckle correlation time.

The goal of this study was to evaluate the use of two velocity distribution assumptions to calculate SFI [6]. To achieve this goal, we employed Mandel's definition of correlation time [20].

2. Lorentzian and Gaussian velocity distributions

When coherent light is used to illuminate an object, a speckle pattern is evident. If the object contains moving optical scatterers (i.e., red blood cells), the speckles will fluctuate in time. A time-integrated image will show a reduction in the speckle contrast due to averaging of the intensity of each speckle. This reduction in contrast is related to the flow velocity. The higher the velocity, the faster the intensity fluctuations, and therefore, the larger the reduction in contrast that occurs over a given exposure time.

Based on speckle statistics, Fercher and Briers [5] derived the following relationship between the speckle contrast (C) and the normalized autocorrelation function of the remitted light:

$$C^2 = \sigma^2 / \langle I \rangle^2 = (1/T) \int_0^T |\gamma(t)|^2 dt \quad (1)$$

where σ is the variance, $\langle I \rangle$ is the mean and $\gamma(t)$ is the normalized autocorrelation function of the remitted light. For a Lorentzian velocity distribution:

$$|\gamma(t)| = \exp(-|t|/\tau_c), \quad (2)$$

Substitution of Eq. 2 into Eq. 1 yields [5]:

$$C = \{(\tau_c / 2T)[1 - \exp(-2T/\tau_c)]\}^{1/2} \quad (3)$$

Briers et al. [22] performed a similar analysis for a Gaussian velocity distribution assumption, obtaining:

$$C = \left[\left(\pi^{1/2} / 2 \right) (\tau_c / T) \operatorname{erf} (T / \tau_c) \right]^{1/2} \quad (4)$$

We postulate that Briers et al. employed the following expression for the normalized autocorrelation function representing a Gaussian velocity distribution:

$$|\gamma(t)| = \exp(-t^2 / 2\tau_c^2), \quad (5)$$

Substitution of Eq 5 into Eq. 1 yields Eq 4.

Figure 1 demonstrates that the use of the two velocity distribution assumptions result in different SFI values ($\text{SFI} = 1/\tau_c \propto$ blood flow velocity) for given values of C . Moreover, for $T/\tau_c > 2$, Eqs 3 and 4 can be simplified to the following algebraic expressions:

$$\begin{aligned} \tau_{cl} &= 2TC^2 \\ \tau_{cg} &= 2TC^2 / (\pi^{1/2}) \end{aligned} \quad (6)$$

where τ_{cl} and τ_{cg} are the correlation times for the Lorentzian and Gaussian approximations, respectively. This result is in agreement with the simplified imaging equation obtained by Cheng and Duong [18].

From Eq 6:

$$1/\tau_{cg} = (\pi^{1/2}) (1/\tau_{cl}) \quad (7)$$

suggesting that for $T/\tau_c > 2$, the velocity predicted by the Gaussian approximation is $\sqrt{\pi}$ times the velocity predicted by the Lorentzian approximation.

In Ref [6], the authors developed an experiment for which the actual decrease in the computed speckle contrast was from 0.15 to 0.01. Adopting the Lorentzian model (Eq. 3) the authors obtained an approximated velocity change from 55 to 120 $\mu\text{m/s}$ and adopting the Gaussian model (Eq. 4), it suggested a velocity change from 100 to 200 $\mu\text{m/s}$; this discrepancy is predicted by the Eq. 7. These results, obtained by Briers et al [6], suggest that the velocity distribution model does impact the relationship between speckle contrast and τ_c . In the next paragraphs we re-derived an equation for the Gaussian model to address the

discrepancy mentioned above and demonstrate that the mapping can indeed differ at high speckle contrast values, but for the large majority of speckle contrast values (0 to 0.6) encountered in practice, the two velocity distributions result in identical mapping between speckle contrast and τ_c .

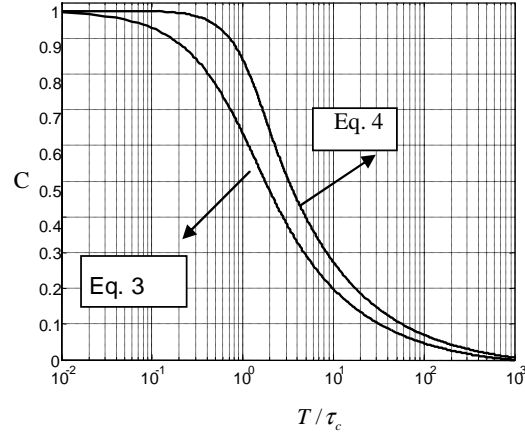


Fig 1. Use of either Lorentzian and Gaussian velocity distributions (Eqs. 3 and 4 respectively) result in distinct relationships between C and the ratio T/τ_c (which is proportional to SFI)

3. Rederived Gaussian equation

In many applications it is desirable to have a precise definition of the term “correlation time”. Such a definition can be made in terms of $\gamma(t)$, but there are different expressions of $\gamma(t)$ reported in the literature [23]. We employed Mandel’s definition of the correlation time:

$$\tau_c = \int_{-\infty}^{\infty} |\gamma(t)|^2 dt \quad (8)$$

It is straightforward to show that Eq 2 satisfies Eq 8, but Eq 5 does not. To address this discrepancy, we propose an alternate expression for the Gaussian normalized autocorrelation function:

$$|\gamma(t)| = \exp(-\pi^2 / 2\tau_c^2) \quad (9)$$

which satisfies Eq. 8. Substituting Eq. 9 into Eq. 1, we obtain:

$$C = \left[(1/2)(\tau_c / T) \operatorname{erf}(\pi^{1/2} T / \tau_c) \right]^{1/2} \quad (10)$$

which is similar to Eq. 4. Furthermore, the argument of the error function in Eq. 10 is similar to that described previously by Goodman (Eq. 6.1-20 in [20]) for a Gaussian spectral profile.

For $T/\tau_c > 2$, Eq. 10 becomes:

$$\tau_{cga} = 2TC^2 \quad (11)$$

where τ_{cga} is the correlation time for the re-derived Gaussian-based speckle imaging equation. Note that this equation is identical to that derived using the more common Lorentzian velocity distribution assumption (Eq. 6, top row).

Thus, when the normalized autocorrelation function for the Gaussian and Lorentzian velocity distributions satisfy the same definition for the correlation time (Eq. 8), then both approximations predict the same SFI values for low C values (Fig. 2, $0 < C < 0.6$).

For $T/\tau_c \ll 1$, Eqs. 3 and 10 can be approximated as

$$\begin{aligned} T/\tau_{cl} &= (1 - C^2) \\ T/\tau_{cga} &= (3/\pi)^{1/2} (1 - C^2)^{1/2} \end{aligned} \quad (12)$$

demonstrating that use of either the Lorentzian or rederived Gaussian velocity distribution assumption predict different τ_c (and hence SFI) values. Although $T/\tau_c \ll 1$ is not encountered in typical LSI experiments, Eq. 12 demonstrates that only in this range of ratios ($T/\tau_c \ll 1$) will the velocity distribution assumption affect the mapping between speckle contrast and τ_c .

From Goodman's theory on integrated intensity [20], which takes into account the *triangular averaging* of the correlation function [19], it is straightforward to obtain:

$$C = \left[(\tau_{c_{lg}}/T) + (1/2)(\tau_{c_{lg}}/T)^2 \left[\exp(-2T/\tau_{c_{lg}}) - 1 \right] \right]^{1/2} \quad (13)$$

and

$$C = \left((\tau_{c_{gg}}/T) \operatorname{erf}(\pi^{1/2} T/\tau_{c_{gg}}) - (1/\pi)(\tau_{c_{gg}}/T)^2 \left[1 - \exp\left[-\pi(T/\tau_{c_{gg}})^2\right] \right] \right)^{1/2}, \quad (14)$$

where $\tau_{c_{lg}}$ and $\tau_{c_{gg}}$ are the correlation times for the Lorentzian and Gaussian approximations, respectively. For $T/\tau_c > 2$, Eqs. 13 and 14 can be simplified to the following expressions:

$$1/\tau_{c_{lg}} = 1/TC^2 = 1/\tau_{c_{gg}} \quad (15)$$

The relationship between $\tau_{c_{lg}}$ and C is similar to that derived by Cheng and Duong [18].

Once again, Eq. 15 suggests that for $T/\tau_c > 2$ (i.e., $0 < C < 0.6$, see Fig. 2), Goodman's theory predicts the same SFI range for the Lorentzian and Gaussian velocity distributions. Moreover, from Eqs. 6 (top row), 11 and 15, the SFI values predicted by Goodman's model are directly proportional to the Lorentzian and the rederived Gaussian-based speckle imaging equations.

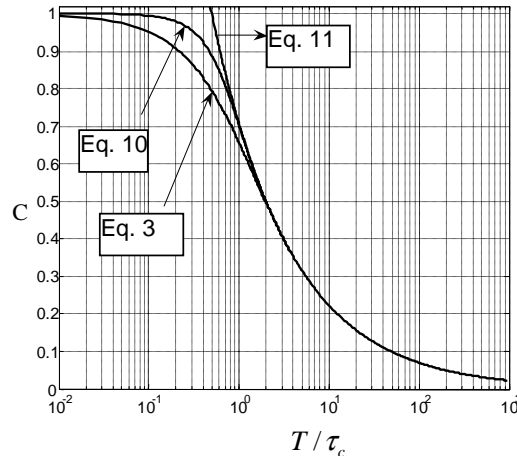


Fig. 2. Use of either Lorentzian and rederived Gaussian speckle imaging equations (Eqs. 3 and 10 respectively) results in identical mapping of C to the ratio T/τ_c for $0 < C < 0.6$.

In Ref [20], the signal-to-noise ratio associated with measurement of $(1/C^2)$ is given by:

$$(S/N)_{rms} = \sqrt{T/\tau_c} . \quad (16)$$

The $(S/N)_{rms}$ associated with Eq. 15 is greater than $\sqrt{2}$. At higher ($C > 0.6$) speckle contrast values, $(S/N)_{rms}$ is less than $\sqrt{2}$, which is unacceptably low for practical application. Eq. 16 is valid for both the Briers and Goodman models.

Briers et al. [6] first noted that experimental C values did not reach the theoretical limit of unity for completely stationary objects; they instead observed a maximum value of 0.6. Experimental data from Yuan et al. [10] also achieved a maximum C value of 0.6. Dunn et al. [1] and Bolay et al. [12] presented experimental data taken from cortical tissue with maximum C values of ~ 0.15 . In experimental LSI data that we acquire from rodent dorsal window chamber models [15-17], we typically observe C values greater than 0.6 in less than 1% of the pixels (Fig. 3). It is important to note that measured C values may differ among LSI instruments due to differences in parameters such as quality of imaging optics and camera, coherence length of incident light source, etc. Nevertheless, we believe these studies collectively justify the rationale for other researchers employing LSI to utilize the proposed simplified speckle imaging equation (Eq. 15). An advantage of Eq. 15 over either use of approximate solutions or look-up tables to extract τ_c from the speckle imaging equation is that it represents an exact analytical solution for $C < 0.6$.

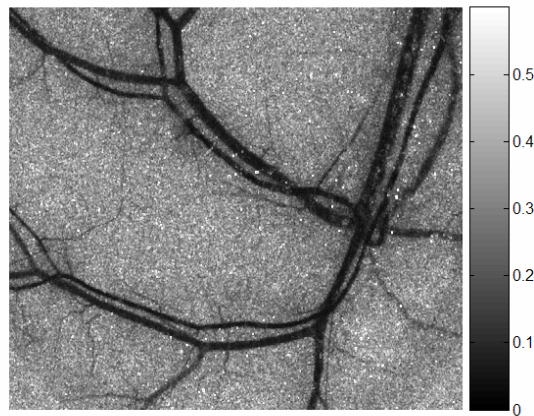


Fig 3. Representative speckle contrast image of a microvascular network in a rodent dorsal skinfold window chamber model. Of the ~ 1.4 million pixels comprising the image, only 2718 ($\sim 0.2\%$) of the pixels have C values greater than 0.6.

Cheng and Duong [18] stated that typically-encountered ratios of T/τ_c are 100 to 400. Values greater than 100 are encountered in clearly defined blood vessels, but the ratio is much lower for pixels that map to poorly-perfused regions of tissue. For example, a speckle contrast of 0.6, which is encountered experimentally, maps to a ratio of two. Our analysis demonstrates that, even for such a low ratio, the simplified imaging algorithm can be used with high accuracy.

4. Conclusions

When the normalized autocorrelation function for the Lorentzian and Gaussian velocity distributions satisfy the same definition of correlation time, the same SFI values are predicted for low contrast ($0 < C < 0.6$) conditions and different values predicted for high contrast conditions. A similar trend is predicted by Goodman's model. Previously, the only ways to

extract τ_c from the imaging equation involved either an approximate solution to or use of look-up tables. Based on our own unpublished experimental data, we have shown that a simplified speckle imaging equation (Eq. 15) will cover the vast majority of practical experimental conditions.

Acknowledgements

The authors acknowledge financial support from the Arnold and Mabel Beckman Foundation; a CONACyT-Mexico Grant (49573-2006, to JCRSJ); National Institutes of Health Laser Microbeam and Medical Program (LAMMP), a NIH Biomedical Technology Resource, Grant No. P41-RR01192, at the University of California, Irvine; and the Whitaker Foundation. The authors thank Mr. Justin Lotfi, Beckman Laser Institute, University of California, Irvine, for the raw speckle imaging data used for Fig 3.